Improved Calibration Technique for Quasi-Monostatic Polarimetric Measurement System Using a Dihedral as the Calibration Reference

Pengfei Wu and Xiaojian Xu

***Abstract*— The alluring polarimetric characteristics of a dihedral corner reflector make it specially useful as a polarimetric calibration reference. However, for a radar cross section (RCS) range with quasi-monostatic geometry where there exists a small bistatic angle, the polarimetric calibration error rapidly increases as the bistatic angle increases when a dihedral is used as the polarimetric calibration reference. In this work, an improved calibration technique for quasi-monostatic polarimetric measurement system is proposed. The scattering mechanism of a rectangular dihedral corner reflector in a quasi-monostatic radar system is analyzed, where the bistatic angle constrains to be within a few degrees. The polarimetric characteristic of the dihedral is evaluated by means of physical optics (POs) approximation. Combining the evaluation formulation with a nonlinear calibration technique, the polarimetric measurement error model can be adapted for the quasi-monostatic geometry so that accurate polarimetric calibration may be accomplished. The experimental results are presented to validate the proposed technique with essential improvement in the calibrated cross polarimetric measurements.**

***Index Terms*— Calibration, dihedral corner reflector, polarimetric calibration, quasi-monostatic, radar cross section (RCS).**

I. Introduction

THE problem of polarimetric calibration for monostatic measurement geometry has been widely studied. Since 1990s, the standard RST model [1] has been introduced to describe the errors of polarimetric measurement including the channel imbalances and antenna crosstalk. Wiesbeck and Riegger [1], Wiesbeck and Kahny [2], Sarabandi and Ulaby [3], and Nashashibi *et al.* [4] proposed different calibration techniques to obtain the accurate polarimetric scattering matrix (PSM) of targets for specific radar systems. Among others, much of the published works used a dihedral corner reflector as the calibration reference, such as the rectangular-shaped dihedral was used by Chen *et al.* [5], Unal *et al.* [6], and Muth [7], [8] and the triangular-shaped dihedral was used by Gau and Burnside [9] and Welsh *et al.* [10].

In many radar cross section (RCS) ranges, the measurement geometry is quasi-monostatic where the transmitting antenna and receiving antenna are separated with a small distance, i.e., the measurement geometry is bistatic where the bistatic angle constraints to a few degrees. As is well known, the bistatic RCS approaches to the monostatic RCS when the bistatic angle is small [11]. However, the difference between monostatic [12], [13] and bistatic [14]–[17] RCSs of dihedral will result in additional calibration error. As a consequence, for accurate polarimetric calibration, quasi-monostatic correction must be made.

The objective of this study is to develop and recommend a modified polarimetric calibration procedure that can be used to correct the bistatic scattering error term of a dihedral for quasi-monostatic measurement geometries. This work is an essential extension of our previous conference paper on ICEAA 2016 [18], where the scattering mechanisms of a rectangular dihedral reflector with both monostatic and quasi-monostatic measurement geometries were analyzed and a correction formulation was proposed by taking the physical optics (POs) solution of a metal plate as reference. In this paper, we present a detailed formulation based on analytic POs (APOs) [19], [20] for quasi-monostatic scattering of a rectangular dihedral rotating around radar line of sight (LOS). Using the derived formulation, the polarimetric measurement error model of dihedral with monostatic geometry is adapted to quasi-monostatic geometry. The system parameters are then obtained by means of Fourier analysis [7], [8], with more accurate polarimetric calibration being accomplished. Finally, the experimental results are presented to validate the proposed calibration technique, demonstrating essential improvement in the cross polarimetric measurements.

The remainder of this paper is organized as follows. The error model of polarimetric measurement and calibration technique with monostatic geometry are briefly described in Section II. In Section III, the scattering mechanisms of dihedral reflector with quasi-monostatic geometry are analyzed and the evaluation formulation of the error caused by small bistatic angle is developed. The measurement error model of polarimetric calibration with quasi-monostatic geometry is

Manuscript received October 15, 2018; revised May 27, 2019; accepted June 8, 2019. Date of publication July 18, 2019; date of current version October 29, 2019. This work was supported by the National Natural Science Foundation of China under Grant 61371005. *(Corresponding author: Xiaojian Xu.)*

The authors are with the School of Electronics and Information Engineering, Beihang University, Beijing 100191, China (e-mail:wupengfeibbi@sina.com; xiaojianxu@buaa.edu.cn).

Color versions of one or more of the figures in this article are available online at http://ieeexplore.ieee.org.

Digital Object Identifier 10.1109/TAP.2019.2927877

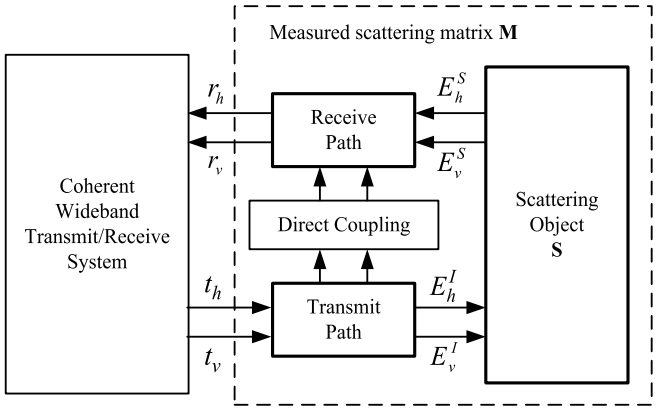

Fig. 1. Schematic block diagram of a polarimetric RCS measurement system.

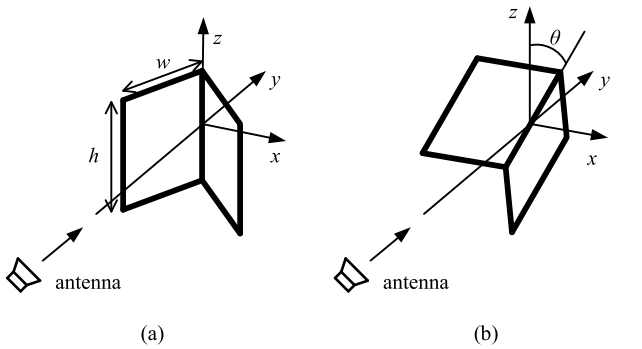

Fig. 2. Dihedral reflector with monostatic measurement geometry. (a) 0 rotation angle. (b) θ rotation angle.

discussed in Section IV, with a modified calibration technique being proposed for enhanced accuracy. The measurement and calibration results are presented in Section V with analysis to validate the proposed technique. We summarize this paper in Section VI.

II. Polarimetric Calibration Technique for Monostatic Geometries

Quite a few papers have been published that discuss the procedures performing full polarimetric calibration from radar PSM measurement. These procedures generally deal with systematic and linear errors. Statistical errors may be reduced by averaging over several measurement cycles. In the case considered, the orthogonal polarizations are linearly horizontal and vertical. The typical schematic block diagram used to describe the polarimetric measurement system is given in Fig. 1 [1], [2].

The measurement equipment has no direct mutual coupling with the target. The object's scattering characteristic is represented using a complex PSM $\begin{bmatrix} S_{hh} & S_{hv} \\ S_{vh} & S_{vv} \end{bmatrix}$, which is related to the measured matrix $\begin{bmatrix} M_{hh} & M_{hv} \\ M_{vh} & M_{vv} \end{bmatrix}$ by

$$\begin{bmatrix} M_{hh} & M_{hv} \\ M_{vh} & M_{vv} \end{bmatrix} = \begin{bmatrix} R_{hh} & R_{hv} \\ R_{vh} & R_{vv} \end{bmatrix} \cdot \begin{bmatrix} S_{hh} & S_{hv} \\ S_{vh} & S_{vv} \end{bmatrix} \cdot \begin{bmatrix} T_{hh} & T_{hv} \\ T_{vh} & T_{vv} \end{bmatrix} + \begin{bmatrix} I_{hh} & I_{hv} \\ I_{vh} & I_{vv} \end{bmatrix} \quad (1)$$

where $\begin{bmatrix} T_{hh} & T_{hv} \\ T_{vh} & T_{vv} \end{bmatrix}$ and $\begin{bmatrix} R_{hh} & R_{hv} \\ R_{vh} & R_{vv} \end{bmatrix}$ are the distortion matrices for transmitting and receiving, respectively. Matrix $\begin{bmatrix} I_{hh} & I_{hv} \\ I_{vh} & I_{vv} \end{bmatrix}$ denotes the isolation errors of direct coupling path. Thus, the measured matrix is subject to 12 error components. The determination of the coefficients in $\begin{bmatrix} I_{hh} & I_{hv} \\ I_{vh} & I_{vv} \end{bmatrix}$ is simply performed by an isolation measurement (empty room) for which $\begin{bmatrix} S_{hh} & S_{hv} \\ S_{vh} & S_{vv} \end{bmatrix} = \begin{bmatrix} 0 & 0 \\ 0 & 0 \end{bmatrix}$ by definition. After the vector background subtraction of isolation errors, the measured matrix can be normalized by the copolarization channels and rewritten as

$$\begin{bmatrix} M_{hh} & M_{hv} \\ M_{vh} & M_{vv} \end{bmatrix} = \begin{bmatrix} R_{hh} & 0 \\ 0 & R_{vv} \end{bmatrix} \cdot \begin{bmatrix} 1 & \varepsilon_h^r \\ \varepsilon_v^r & 1 \end{bmatrix} \cdot \begin{bmatrix} S_{hh} & S_{hv} \\ S_{vh} & S_{vv} \end{bmatrix} \cdot \begin{bmatrix} 1 & \varepsilon_v^t \\ \varepsilon_h^t & 1 \end{bmatrix} \cdot \begin{bmatrix} T_{hh} & 0 \\ 0 & T_{vv} \end{bmatrix} \quad (2)$$

where $\varepsilon_h^r = R_{hv}/R_{hh}$, $\varepsilon_v^r = R_{vh}/R_{vv}$,$\varepsilon_h^t = T_{vh}/T_{hh}$, and $\varepsilon_v^t = T_{hv}/T_{vv}$ are the cross-polarimetric coefficients of receiving and transmitting channels. The determination of these unknowns is based on the measurement of calibration references for which the PSMs are well known. In [1]–[10], different approaches for the calculation of the system error coefficients are shown.

The dihedral corner reflector is used as calibration reference in many calibration techniques. For a monostatic measurement geometry, the different orientations of a rectangular dihedral reflector [2] are shown in Fig. 2(a) and (b).

It is noted that in Fig. 2, the y-axis is along the radar LOS. The x- and z-axes are the two cross-range coordinates. The two plates form the dihedral intersect at 90° and both of them are rectangles with w in width and h in height. The direction of the incident electromagnetic wave is perpendicular to the aperture of the dihedral. When the dihedral is rotated with an angle of θ about the LOS, as shown in Fig. 2(b), at high frequencies, the theoretical PSM of the dihedral (neglecting diffraction) is [8]

$$\begin{bmatrix} S_{hh} & S_{hv} \\ S_{vh} & S_{vv} \end{bmatrix} = S_{dih} \begin{bmatrix} -\cos 2\theta & \sin 2\theta \\ \sin 2\theta & \cos 2\theta \end{bmatrix} \quad (3)$$

where $S_{dih} = \sqrt{2}\ wh/\lambda$, which depends on the dimensions of the dihedral and is assumed to be known, λ is the radar wavelength.

In most of the polarimetric calibration techniques, the dihedral needs to be measured at two orientations such as with rotation angles of 0° and 45° [2], [5], [9], [10]. In other techniques, more polarimetric calibration data are measured during the dihedral rotation from 0° to 180° [6]–[8]. For the full polarimetric measurements, the measured values can be written as

$$M_{hh} = R_{hh}T_{hh}S_{dih}\left[\left(\varepsilon_h^r\varepsilon_h^t - 1\right)\cos 2\theta + \left(\varepsilon_h^r + \varepsilon_h^t\right)\sin 2\theta\right] \quad (4)$$

$$M_{hv} = R_{hh}T_{vv}S_{dih}\left[\left(\varepsilon_h^r - \varepsilon_v^t\right)\cos 2\theta + \left(1 + \varepsilon_h^r\varepsilon_v^t\right)\sin 2\theta\right] \quad (5)$$

$$M_{vh} = R_{vv}T_{hh}S_{dih}\left[\left(\varepsilon_h^t - \varepsilon_v^r\right)\cos 2\theta + \left(1 + \varepsilon_v^r\varepsilon_h^t\right)\sin 2\theta\right] \quad (6)$$

$$M_{vv} = R_{vv}T_{vv}S_{dih}\left[\left(1 - \varepsilon_v^r\varepsilon_v^t\right)\cos 2\theta + \left(\varepsilon_v^r + \varepsilon_v^t\right)\sin 2\theta\right]. \quad (7)$$

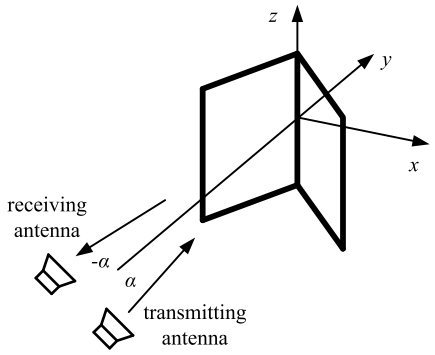

Fig. 3. Dihedral with quasi-monostatic measurement geometry.

The matrix elements for all the polarization combinations have the general form

$$M_{pq} = c_{pq}\cos 2\theta + s_{pq}\sin 2\theta \tag{8}$$

where p and q are either h or v. We applied Fourier analysis to the data to determine the cross-polarimetric coefficients. Actually, there are some noises and errors that hardly be removed more or less in measurement. As a consequence, the measurement can then be expressed as the Fourier series

$$M = C_0 + c_1\cos\theta + s_1\sin\theta + c_2\cos\ 2\theta + s_2\sin 2\theta + c_3\cos\ 3\theta + s_3\sin 3\theta + \cdots. \tag{9}$$

Mathematically, the signals of dihedral correspond to the coefficients c_2 and s_2, respectively. They are used to determine the cross-polarimetric coefficients, and others such as c_1 and s_1 are omitted in polarimetric calibration procedure. Because the background is stationary, the contributions of the background and noises to the dihedral signals are greatly reduced. The details of the theoretical expressions have been presented in [7] and [8]. With the measurement results of another calibration reference, all polarimetric error coefficients can be solved and the polarimetric calibration can be accomplished.

III. Formulation of Bistatic Correction With Quasi-Monostatic Geometry

Many RCS ranges have quasi-monostatic measurement geometries where two antennas are used for transmitting and receiving, as shown in Fig. 3. Here, suppose that the transmitting antenna is set on the right side, while the receiving antenna is set on the left. It is seen that the incidence angle (half of the bistatic angle) is α and the scattering angle is $-\alpha$, which are related to the locations of the antennas and the dihedral, while independent of the dihedral rotation and the polarization of the electromagnetic wave.

The small bistatic angle leads to the differences in scattering mechanisms between monostatic and quasi-monostatic geometries. Because of the special structure of dihedral reflector, the double reflection from the plates of the dihedral is the major scattering component during polarimetric calibration, which the electromagnetic wave reflect from one plate to another and then back in the scattering direction. Other components contributing to the scattered field are weaker than the double reflection component [12]. The differences in double reflections between monostatic and quasi-monostatic geometries are analyzed in detail.

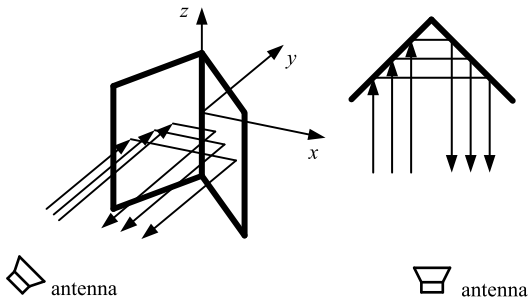

Fig. 4. Dihedral with rotation angle of 0° for monostatic measurement geometry.

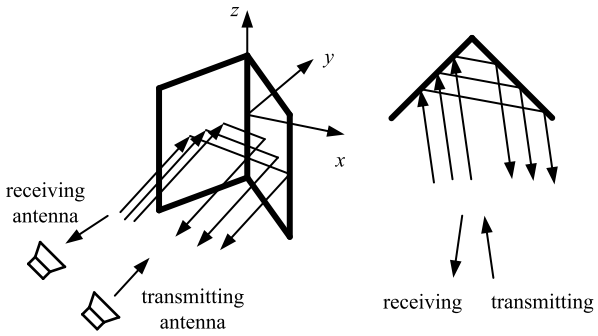

Fig. 5. Dihedral with rotation angle of 0° for quasi-monostatic measurement geometry.

A. Dihedral With Rotation Angle of 0°

Figs. 4 and 5 illustrate the scattering mechanisms of dihedral reflector with rotation angle of 0° for monostatic and quasi-monostatic measurement geometries, respectively.

For monostatic measurement geometry, the incidence direction is normal sight, and the incidence angle equals to zero. The scattering direction of double reflection is parallel to the incidence direction so that it is right along the observing direction (LOS to the receiving antenna). For quasi-monostatic geometry, as shown in Fig. 5, there is a misalignment between the scattering direction and the observing direction. The misalignment causes loss of energy received by antenna, which in other words is bistatic magnitude correction term.

The scattering mechanism of a dihedral is similar to metal plate except that double reflections must be considered [21]. Therefore, the metal plate with the same aperture size as the dihedral is analyzed to evaluate the bistatic correction term. Specifically, the metal plate is $\sqrt{2}\ w$ in width and h in height.

Fig. 6 shows the monostatic measurement geometry which irradiated in normal sight and incidence angle equals to zero. The scattering direction is similar to the dihedral with monostatic geometry. Fig. 7 demonstrates the monostatic geometry with a small incidence angle. The incidence direction tilts a minus angle in horizontal, and the misalignment between scattering and observing directions occurs. It is similar to the dihedral with quasi-monostatic geometry. So, we use it to evaluate the bistatic correction term of dihedral.

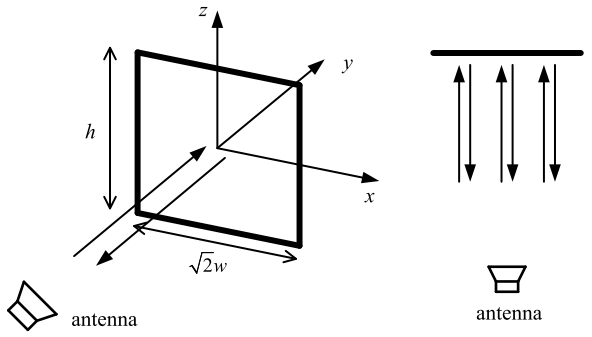

Fig. 6. Metal plate in normal sight with monostatic geometry.

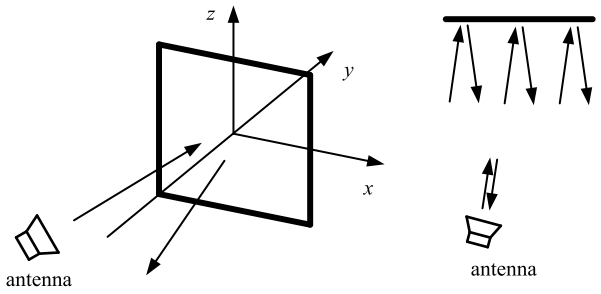

Fig. 7. Metal plate with a small incidence angle.

According to the PO solution, the RCS of metal plate is [21]

$$\sigma(\varphi) = \frac{4\pi}{\lambda^2} a^2 b^2 \cos^2\varphi \left[\frac{\sin(ka\sin\varphi)}{ka\sin\varphi}\right]^2 \tag{10}$$

where a and b are the width and height of the metal plate, respectively, φ is the incidence angle, and $k = 2\pi/\lambda$ is the wavenumber. Compared with the normal sight situation, the correction term can be written as

$$\frac{\sigma(\varphi)}{\sigma(0)} = \cos^2\varphi \left[\frac{\sin(ka\sin\varphi)}{ka\sin\varphi}\right]^2. \tag{11}$$

The bistatic scattering of the dihedral corner reflector can be calculated by APO [19]. As the quasi-monostatic geometry shown in Fig. 3, the APO solution can be approximated and simplified in small bistatic angle cases. A detailed derivation can be found in the Appendix. The correction term is given by (A10) in the Appendix and is duplicated here for convenience

$$l_{PSM}(\alpha) = \left|\cos\alpha \left[\frac{\sin(k\sqrt{2}w\sin\alpha)}{k\sqrt{2}w\sin\alpha}\right]\right|. \tag{12}$$

It can be easily seen that the quasi-monostatic correction term of dihedral is the same as the correction term of plate, demonstrating the scattering mechanisms we analyzed. The bistatic RCS correction term of the dihedral reflector with rotation angle of 0° is

$$l_{RCS}(\alpha) = \cos^2\alpha \left[\frac{\sin(k\sqrt{2}w\sin\alpha)}{k\sqrt{2}w\sin\alpha}\right]^2. \tag{13}$$

B. Dihedral With Rotation Angle of 90°

The scattering mechanism of dihedral with rotation angle of 90° is shown in Fig. 8.

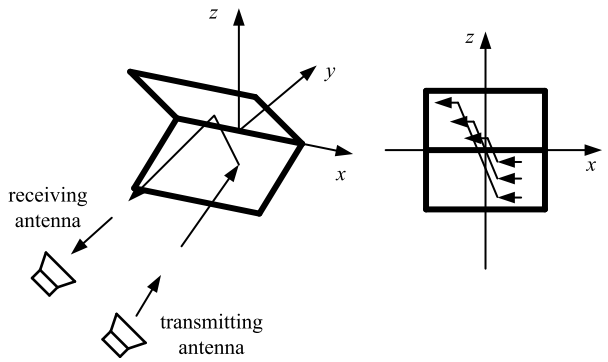

Fig. 8. Dihedral with rotation angle of 90° for quasi-monostatic measurement geometry.

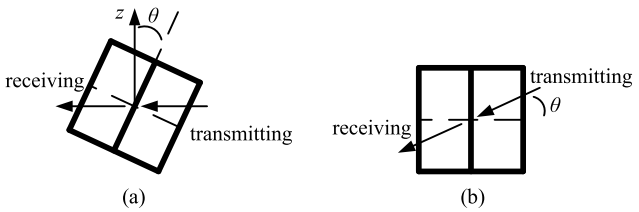

Fig. 9. Dihedral with rotation angle of $\theta$for quasi-monostatic measurement geometry. (a) Front view. (b) Equivalent situation.

The front view shows the double reflection of dihedral with quasi-monostatic geometry clearly. It can be easily seen that, in this situation, the scattering direction is the same as the observing direction. The RCS of dihedral is impacted by the reduction of effective illumination region. It can be omitted when the incidence angle approaches 0°.

C. Other Cases

Finally, we think about the situation of rotation angle that is neither 0° nor 90°. Fig. 9(a) shows the dihedral with rotation angle of θ with quasi-monostatic geometry.

Suppose that the dihedral is rotated from θ to 0° case. In order to keep the scattering characteristics unchanged, the locations of the antennas are rotated simultaneously with the bistatic angle fixed. It is shown in Fig. 9(b) as the equivalent situation. The orientation of the dihedral is the same as that in the work of Jackson [19]; however, the polarization directions of electromagnetic waves are different. As a consequence, the scattering characteristics should be recalculated or revised on the basis of reference. According to (12), after small angle approximation, the bistatic correction term is not related to the polarization. Therefore, the bistatic angle can be decomposed to azimuth angle in horizontal and elevation angle in vertical. The bistatic correction term in horizontal is the same as 0° case and the azimuth angle is $\alpha\cos\theta$. The bistatic correction term in vertical is the same as 90° case, which can be ignored. In summary, when the rotation angle of the dihedral is θ, the bistatic correction term may be approximated by l_{PSM} $(\alpha\cos\theta)$.

IV. Measurement Error Model With Quasi-Monostatic Geometry

In this section, by taking a specific example, we discuss the measurement error model with quasi-monostatic geometry.

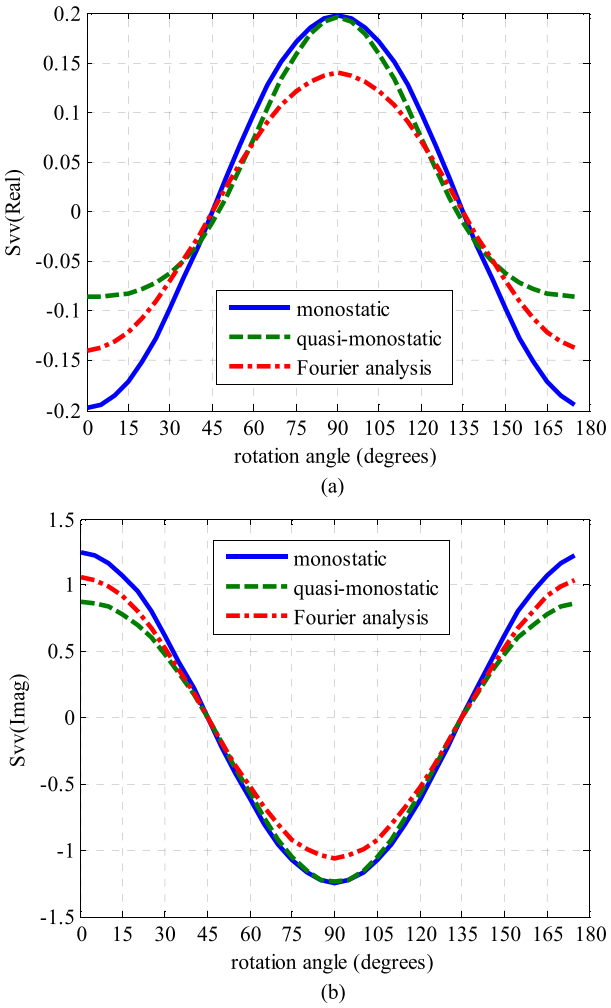

Fig. 10. VV polarization of the dihedral with monostatic geometry, quasi-monostatic geometry with bistatic angle of 4°, and the Fourier analysis result of quasi-monostatic geometry at 10 GHz. (a) Real part. (b) Imaginary part.

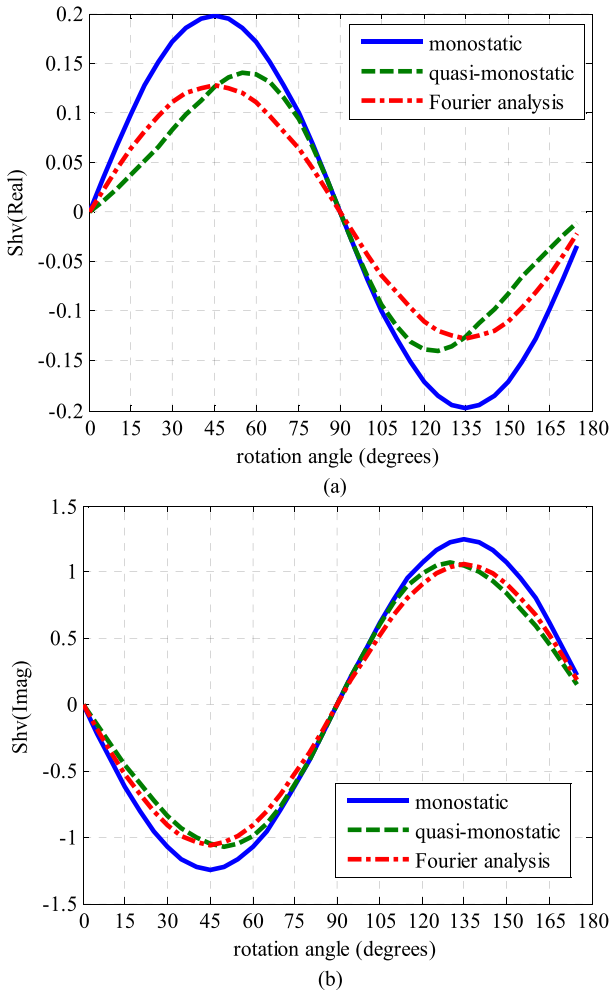

Fig. 11. HV polarization of the dihedral with monostatic geometry, quasi-monostatic geometry with bistatic angle of 4°, and the Fourier analysis result of quasi-monostatic geometry at 10 GHz. (a) Real part. (b) Imaginary part.

We start from the characteristic of a dihedral rotating around the LOS, as shown in Figs. 10 and 11. The PSM of dihedral reflector is calculated using the method of moment (MOM) code of Feko software. The frequency is 10 GHz. Both plates of dihedral are 15 cm in width and 21 cm in height. The angle of incidence is 2° and the angle of observing is −2° for quasi-monostatic geometry. It represents such a case that the space between transmitting and receiving antennas is 50 cm and the target (dihedral) range is 7 m. The dihedral rotates from 0° to 175°, step by 5°. The real and imaginary parts of the vv polarization component are shown in Fig. 10(a) and (b), respectively.

From the numerical result, it can be seen that the bistatic correction term varies with the rotation angle. It is the same as the analysis of scattering mechanisms and the calculation results in Section III. Specifically, when the rotation angle approaches to 0° or 180°, the effect of bistatic angle is strong and the difference between monostatic and quasi-monostatic is obvious. When the rotation angle approaches to 90°, there is little effect of bistatic angle and the difference between monostatic and quasi-monostatic is small.

The formulations in Section III can be applied here to eliminate the bistatic error of quasi-monostatic result, and the Fourier analysis is used to reduce the noise. On the other hand, the Fourier analysis can be applied to the quasi-monostatic result directly and the signal of dihedral can be acquired. It is shown as dot and dashed line in Fig. 10. Because of the bistatic error of dihedral in most of the rotation positions, it can be easily seen that the Fourier component is attenuated when compared with the monostatic result. The attenuation of Fourier analysis result should be estimated and corrected to ensure the accurate polarimetric calibration and it will be discussed in detail.

As the evaluation formulations we get in Section III, the bistatic correction terms of dihedral reflector with rotation angles of 0°, 45°, and 90° are $l_{PSM}\ (\alpha)$,$l_{PSM}\ (\alpha\cos 45°)$, and 1, respectively. For the copolarization, the attenuation of Fourier component is related to the bistatic errors of dihedral with rotation angles of 0° and 90°. Take vv polarization as an example, shown in the Appendix (A25), it will be written as

$$S_{vv,bis} = \frac{l_{PSM}(\alpha)+1}{2} S_{dih} \cos 2\theta. \tag{14}$$

The real and imaginary parts of the hv polarization component are shown in Fig. 11(a) and (b), respectively.

For the cross-polarization, the response of the dihedral with rotation angle of 45° is almost stable during the Fourier analysis. It is used to represent the attenuation of Fourier component. Take hv polarization as an example, shown in the Appendix (A26), it will be written as

$$S_{hv,bis} = l_{PSM}\left(\alpha\cos\frac{\pi}{4}\right) S_{dih}\sin 2\theta. \tag{15}$$

The PSM of dihedral rotating around the LOS can be expressed as

$$S^{\theta}_{dih,bis} = S_{dih} \cdot \begin{bmatrix} -\dfrac{l_{PSM}(\alpha)+1}{2}\cos 2\theta & l_{PSM}\left(\alpha\cos\dfrac{\pi}{4}\right)\sin 2\theta \\ l_{PSM}\left(\alpha\cos\dfrac{\pi}{4}\right)\sin 2\theta & \dfrac{l_{PSM}(\alpha)+1}{2}\cos 2\theta \end{bmatrix}. \tag{16}$$

According to the polarimetric calibration error model, the measurement values of dihedral with quasi-monostatic geometry are

$$M_{hh} = A_{hh}S_{dih}\left[\left(\varepsilon_h^r\varepsilon_h^t-1\right)\frac{l_{PSM}(\alpha)+1}{2}\cos 2\theta + \left(\varepsilon_h^r+\varepsilon_h^t\right)l_{PSM}\left(\alpha\cos\frac{\pi}{4}\right)\sin 2\theta\right] \tag{17}$$

$$M_{hv} = A_{hv}S_{dih}\left[\left(\varepsilon_h^r-\varepsilon_v^t\right)\frac{l_{PSM}(\alpha)+1}{2}\cos 2\theta + \left(1+\varepsilon_h^r\varepsilon_v^t\right)l_{PSM}\left(\alpha\cos\frac{\pi}{4}\right)\sin 2\theta\right] \tag{18}$$

$$M_{vh} = A_{vh}S_{dih}\left[\left(\varepsilon_h^t-\varepsilon_v^r\right)\frac{l_{PSM}(\alpha)+1}{2}\cos 2\theta + \left(\varepsilon_v^r\varepsilon_h^t+1\right)l_{PSM}\left(\alpha\cos\frac{\pi}{4}\right)\sin 2\theta\right] \tag{19}$$

$$M_{vv} = A_{vv}S_{dih}\left[\left(1-\varepsilon_v^r\varepsilon_v^t\right)\frac{l_{PSM}(\alpha)+1}{2}\cos 2\theta + \left(\varepsilon_v^r+\varepsilon_v^t\right)l_{PSM}\left(\alpha\cos\frac{\pi}{4}\right)\sin 2\theta\right] \tag{20}$$

where $A_{hh} = R_{hh}T_{hh}$, $A_{hv} = R_{hh}T_{vv}$, $A_{vh} = R_{vv}T_{hh}$, and $A_{vv} = R_{vv}T_{vv}$ represent the gains of polarimetric channels. Therefore, suppose that the dihedral reflector rotates over 180° or the multiples of 180°, the Fourier component can be calculated easily from the measurements of rotation dihedral. Take the results of hh channel as examples, the Fourier coefficients are

$$c_{hh} = A_{hh}S_{dih}\left[\left(1-\varepsilon_h^r\varepsilon_h^t\right)\frac{l_{PSM}(\alpha)+1}{2}\right] \tag{21}$$

$$s_{hh} = A_{hh}S_{dih}\left[\left(\varepsilon_h^r+\varepsilon_h^t\right)l_{PSM}\left(\alpha\cos\frac{\pi}{4}\right)\right]. \tag{22}$$

The cosine term can be divided from the sine term to eliminate components related to the dihedral and amplification of antennas. A factor which only contains the cross-polarimetric coefficients and bistatic errors will be obtained

$$\frac{s_{hh}}{c_{hh}} = \frac{\left(\varepsilon_h^r+\varepsilon_h^t\right)l_{PSM}\left(\alpha\cos\frac{\pi}{4}\right)}{\left(1-\varepsilon_h^r\varepsilon_h^t\right)\frac{l_{PSM}(\alpha)+1}{2}}. \tag{23}$$

Similarly, for other polarimetric channels, the factors relate to cross-polarimetric coefficients are

$$\frac{c_{hv}}{s_{hv}} = \frac{\left(\varepsilon_v^t-\varepsilon_h^r\right)\frac{l_{PSM}(\alpha)+1}{2}}{\left(1+\varepsilon_h^r\varepsilon_v^t\right)l_{PSM}\left(\alpha\cos\frac{\pi}{4}\right)} \tag{24}$$

$$\frac{c_{vh}}{s_{vh}} = \frac{\left(\varepsilon_v^r-\varepsilon_h^t\right)\frac{l_{PSM}(\alpha)+1}{2}}{\left(\varepsilon_v^r\varepsilon_h^t+1\right)l_{PSM}\left(\alpha\cos\frac{\pi}{4}\right)} \tag{25}$$

$$\frac{s_{vv}}{c_{vv}} = \frac{\left(\varepsilon_v^r+\varepsilon_v^t\right)l_{PSM}\left(\alpha\cos\frac{\pi}{4}\right)}{\left(\varepsilon_v^r\varepsilon_v^t-1\right)\frac{l_{PSM}(\alpha)+1}{2}}. \tag{26}$$

In the four equations above, there are four cross-polarimetric coefficients as unknown components. However, the four equations are not independent of each other, so the cross-polarimetric coefficients cannot be determined. The measurement of other type polarimetric calibration reference is needed, such as the metal plate. The measurement value of a plate can be organized to

$$\frac{M_{hv\ plate}M_{vh\ plate}}{M_{hh\ plate}M_{vv\ plate}} = \frac{\left(\varepsilon_h^r+\varepsilon_v^t\right)\left(\varepsilon_v^r+\varepsilon_h^t\right)}{\left(1+\varepsilon_h^r\varepsilon_h^t\right)\left(1+\varepsilon_v^r\varepsilon_v^t\right)}. \tag{27}$$

We can choose three equations from the results of dihedral and combine with the equation of plate to obtain an equation group, such that the cross-polarimetric coefficients can be solved. According to $|\varepsilon| < 1$ and other limits which are the real situations for most of the RCS system, the true solution can be picked out from the fault solutions.

Then, the gain of each polarimetric channel can be calculated. Take the result of hh polarization as an example, the gain A_{hh} can be expressed as

$$A_{hh} = \frac{c_{hh}}{S_{dih}\left(1-\varepsilon_h^r\varepsilon_h^t\right)}\cdot\frac{2}{l_{PSM}(\alpha)+1}. \tag{28}$$

Till now, the four cross-factors and four channel amplifications of the RCS system are solved out. Finally, the polarimetric calibration of target can be accomplished by

$$S_{hh}^{tar} = \frac{1}{1-\varepsilon_h^t\varepsilon_v^t-\varepsilon_h^r\varepsilon_v^r+\varepsilon_h^r\varepsilon_v^r\varepsilon_h^t\varepsilon_v^t} \times\left(\frac{M_{hh}^{tar}}{A_{hh}}-\varepsilon_h^t\frac{M_{hv}^{tar}}{A_{hv}}-\varepsilon_h^r\frac{M_{vh}^{tar}}{A_{vh}}+\varepsilon_h^r\varepsilon_h^t\frac{M_{vv}^{tar}}{A_{vv}}\right) \tag{29}$$

$$S_{hv}^{tar} = \frac{1}{1-\varepsilon_h^t\varepsilon_v^t-\varepsilon_h^r\varepsilon_v^r+\varepsilon_h^r\varepsilon_v^r\varepsilon_h^t\varepsilon_v^t} \times\left(-\varepsilon_v^t\frac{M_{hh}^{tar}}{A_{hh}}+\frac{M_{hv}^{tar}}{A_{hv}}+\varepsilon_h^r\varepsilon_v^t\frac{M_{vh}^{tar}}{A_{vh}}-\varepsilon_h^r\frac{M_{vv}^{tar}}{A_{vv}}\right) \tag{30}$$

$$S_{vh}^{tar} = \frac{1}{1-\varepsilon_h^t\varepsilon_v^t-\varepsilon_h^r\varepsilon_v^r+\varepsilon_h^r\varepsilon_v^r\varepsilon_h^t\varepsilon_v^t} \times\left(-\varepsilon_v^r\frac{M_{hh}^{tar}}{A_{hh}}+\varepsilon_v^r\varepsilon_h^t\frac{M_{hv}^{tar}}{A_{hv}}+\frac{M_{vh}^{tar}}{A_{vh}}-\varepsilon_h^t\frac{M_{vv}^{tar}}{A_{vv}}\right) \tag{31}$$

$$S_{vv}^{tar} = \frac{1}{1-\varepsilon_h^t\varepsilon_v^t-\varepsilon_h^r\varepsilon_v^r+\varepsilon_h^r\varepsilon_v^r\varepsilon_h^t\varepsilon_v^t} \times\left(\varepsilon_v^r\varepsilon_v^t\frac{M_{hh}^{tar}}{A_{hh}}-\varepsilon_v^r\frac{M_{hv}^{tar}}{A_{hv}}-\varepsilon_v^t\frac{M_{vh}^{tar}}{A_{vh}}+\frac{M_{vv}^{tar}}{A_{vv}}\right). \tag{32}$$

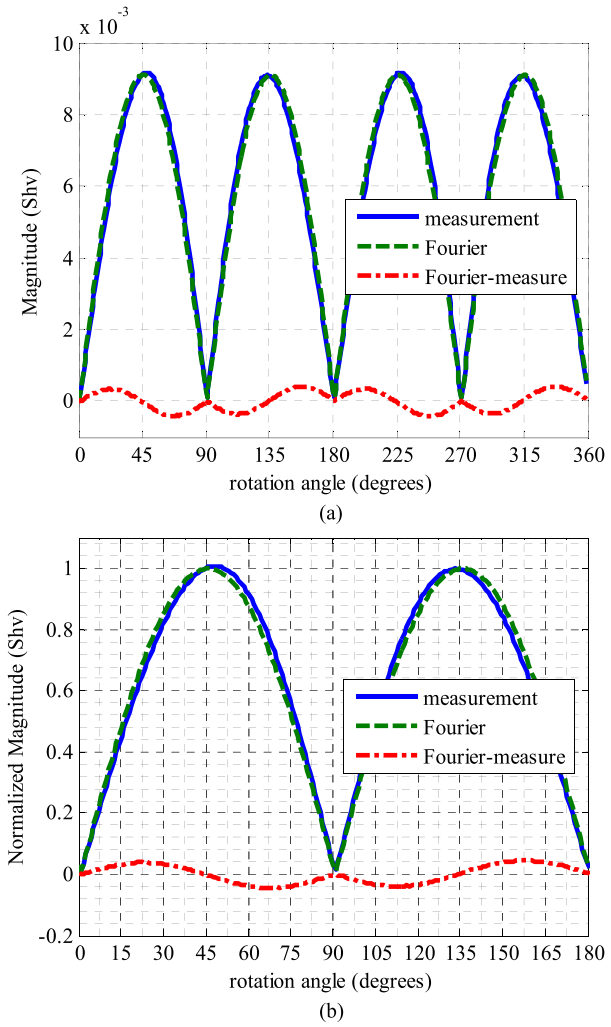

Fig. 12. Measurement (quasi-monostatic and $\alpha = 1.2°$), Fourier result, and deviation of the dihedral varying with rotation angle (hv polarization at 10 GHz). (a) Magnitude. (b) Normalized by the maximum of Fourier result.

V. Experimental Results

We use two rectangular dihedrals and two square metal plates with different size to perform polarimetric calibration in an indoor RCS measurement range. The big dihedral and plate are used as calibration references to calculate the system coefficients. The big dihedral consists of two plates sized 15 cm in width and 21 cm in height, and the square metal plate is 21.5 cm in width. The small dihedral and plate are used as targets whose PSMs are need to be calibrated. The small dihedral consists of two plates sized 7.5 cm in width and 10.5 cm in height, and the square metal plate is 11 cm in width. Scattering measurement is performed using a vector network analyzer (VNA). Time-domain gating technique is applied to remove the possible target-room coupling during the measurement. The space between transmitting and receiving antennas is 19 cm and the target range is 4.5 m that means the bistatic angle α is more than 1.2°.

The measurement, Fourier result, and deviation of the reference dihedral are shown in Fig. 12(a) during the rotation of dihedral at 10 GHz. Altogether, 400 data points were collected for each polarization during a full 360° rotation. In order to eliminate the effect of gains of the system, the results are normalized by the maximum of Fourier result and shown in Fig. 12(b). For an intensive study of the bistatic error,

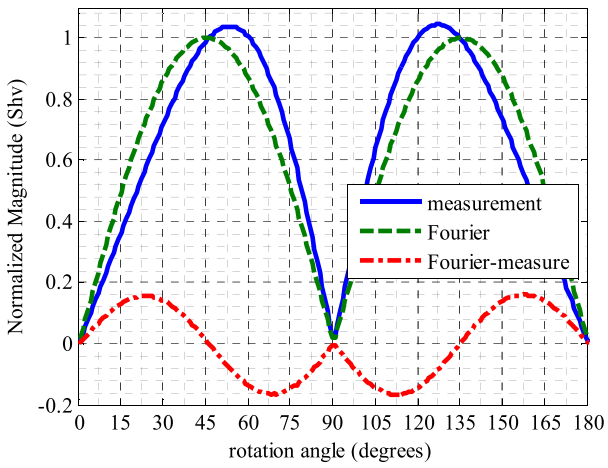

Fig. 13. Normalized results of measurement (quasi-monostatic and $\alpha = 2.5°$), Fourier result, and deviation of the dihedral varying with rotation angle (hv polarization at 10 GHz).

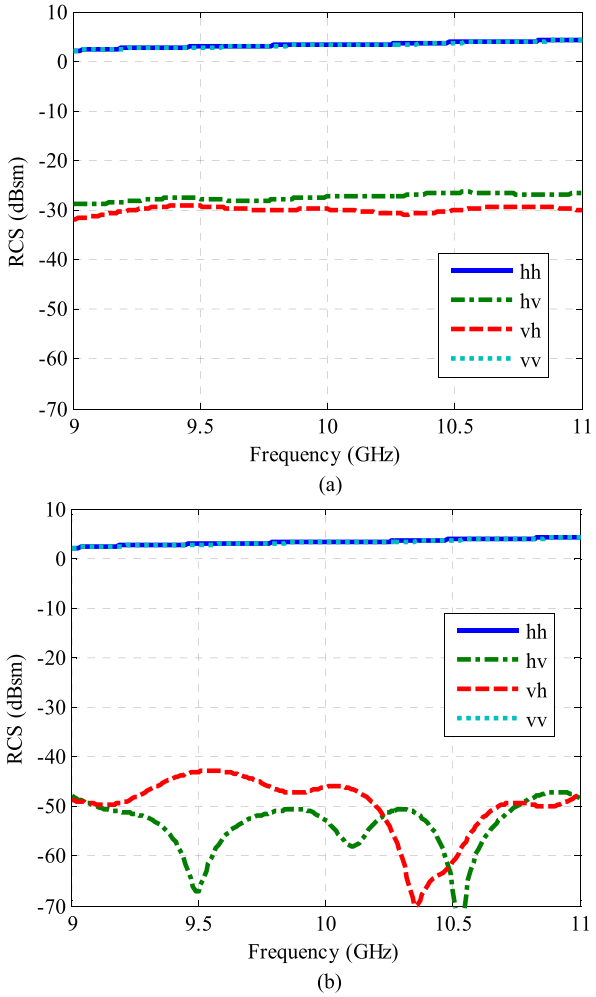

Fig. 14. Full polarimetric measurement results of target metal plate (the square metal plate is 11 cm in width). (a) Before polarimetric calibration. (b) After polarimetric calibration.

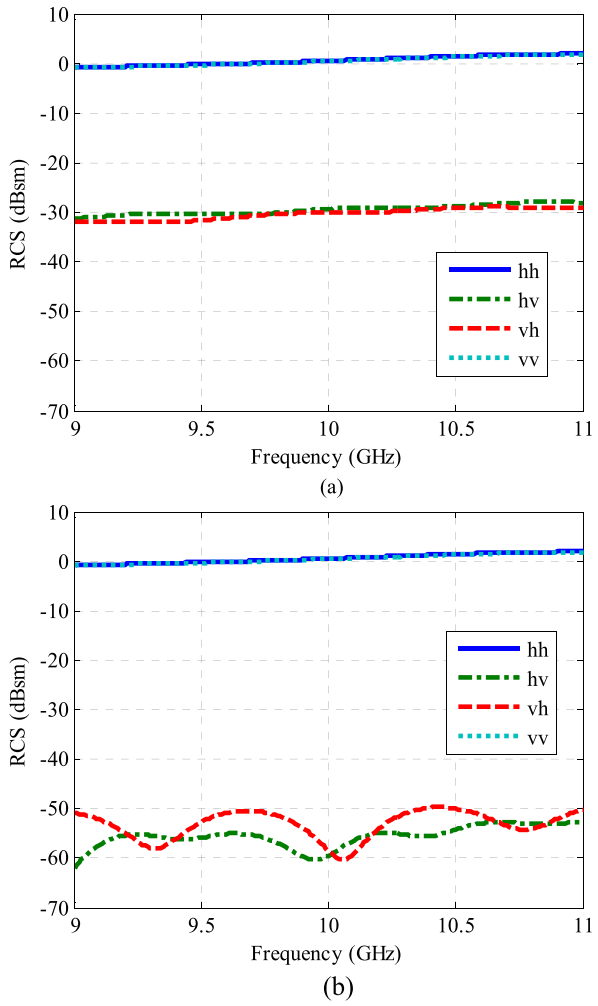

Fig. 15. Full polarimetric measurement results of target dihedral with 0° rotation (both rectangular plates of dihedral are 7.5 cm in width and 10.5 cm in height). (a) Before polarimetric calibration. (b) After polarimetric calibration.

we enlarge the space between transmitting and receiving antennas to 40 cm that means the bistatic angle α is more than 2.5°. The normalized results are presented in Fig. 13.

From Figs. 12(b) and 13, it is found that larger differences do exist at the larger bistatic angle between the measurement (quasi-monostatic) and Fourier results. The bistatic error will cause the attenuation of Fourier component compared with the monostatic result as discussed in Section IV. The measurement results also show that the larger bistatic angles change the shape of curve more obviously.

In Fig. 14(a) and (b), the results of target metal plate before and after polarimetric calibration are illustrated, respectively. It can be seen that the polarization isolation of the measurements is about 30 dB, while after polarimetric calibration, it is as high as about 45 dB.

In Fig. 15(a) and (b), the results of the target dihedral with 0° rotation before and after polarimetric calibration are presented, respectively. The dihedral with 0° rotation is a dominant copolarization target and the cross-polarization component is about 50 dB down from the copolarization component for the calibrated result, 20 dB better than the raw data.

VI. Conclusion

In this work, we proposed an improved polarimetric calibration technique for quasi-monostatic radar system, where the bistatic angle is constrained to be within a few degrees. The polarimetric characteristics of a rectangular dihedral corner reflector rotating around radar LOS in a quasi-monostatic radar system are studied. Based on the analysis of the scattering mechanisms for dihedral with both monostatic and quasi-monostatic measurement geometries, the correction term caused by small bistatic angle is evaluated based on PO approximation. The polarimetric measurement error model is modified for the quasi-monostatic geometry so that accurate polarimetric calibration can be accomplished. By means of the derived formulation, the bistatic error of dihedral reflector can be greatly reduced. The experimental results show that the polarization isolation of calibrated data is well below 45 dB when the bistatic angle α is up to 1.2°. It is, thus, concluded that the proposed technique is useful for more accurate polarimetric calibration with quasi-monostatic measurement geometries, which are very common in RCS test ranges.

Appendix

A. Analytic Physical Optics Solution for Dihedral With Quasi-Monostatic Geometry

The APO solution for bistatic scattering from a dihedral has been excellently calculated by Jackson [19]. The APO result can be simplified according to the quasi-monostatic geometry. Specifically, the two faces of dihedral are the same with w in width, and the directions of both incidence and scattering are in xy plane. Along the LOS, the transmitting antenna is set at the right hand, while the receiving antenna is set at left. That means, for double reflection, the illumination area of dihedral is stable as only a near-boundary stripe at left cannot be illuminated.

For the full polarimetric measurements, the double reflection components of dihedral are

$$S_{vv}(\alpha) = -\frac{jkhw}{\sqrt{\pi}}\left\{\sin\left(\frac{\pi}{4}+\alpha\right)\frac{\sin[Af(\alpha)]}{A}e^{jAf(\alpha)} + \cos\left(\frac{\pi}{4}+\alpha\right)\frac{\sin A}{A}e^{-jA}\right\} \tag{A1}$$

$$S_{vh}(\alpha) = 0 \tag{A2}$$

$$S_{hv}(\alpha) = 0 \tag{A3}$$

$$S_{hh}(\alpha) = \frac{jkhw}{\sqrt{\pi}}\left\{\sin\left(\frac{\pi}{4}-\alpha\right)\frac{\sin[Af(\alpha)]}{A}e^{jAf(\alpha)} + \cos\left(\frac{\pi}{4}-\alpha\right)\frac{\sin A}{A}e^{-jA}\right\} \tag{A4}$$

where

$$f(\alpha) = \frac{1-\tan\alpha}{1+\tan\alpha} \tag{A5}$$

$$A = \frac{\sqrt{2}}{2}kw\sin\alpha. \tag{A6}$$

Considering that the incidence angle α constraints to a few degrees, the value of $f(\alpha)$ can be approximated to 1.

The exponential components in (A1) and (A4) can be written as complex number

$$S_{vv}(\alpha) = -\sqrt{2}\frac{jkhw}{\sqrt{\pi}} \cdot \frac{\sin A}{A}(\cos\alpha \cos A + j \sin\alpha \sin A) \quad \text{(A7)}$$

$$S_{hh}(\alpha) = \sqrt{2}\frac{jkhw}{\sqrt{\pi}} \cdot \frac{\sin A}{A}(\cos\alpha \cos A - j \sin\alpha \sin A). \quad \text{(A8)}$$

Similarly, the value of $\sin\alpha \sin A$ can be approximated to 0 as α is a small angle. The double reflection components of dihedral can be simplified as

$$|S_{vv}(\alpha)| = |S_{hh}(\alpha)| = \left|\cos\alpha \frac{kh\sqrt{2}w}{\sqrt{\pi}} \cdot \frac{\sin 2A}{2A}\right|. \quad \text{(A9)}$$

Comparing the quasi-monostatic result $|S(\alpha)|$ with the monostatic result $|S(0)|$, the correction term is

$$l_{PSM}(\alpha) = \frac{|S(\alpha)|}{|S(0)|} = \left|\cos\alpha \left[\frac{\sin(k\sqrt{2}w \sin\alpha)}{k\sqrt{2}w \sin\alpha}\right]\right|. \quad \text{(A10)}$$

B. Fourier Analysis for Rotating Dihedral With Quasi-Monostatic Geometry

When the dihedral rotates about the LOS, the quasi-monostatic result can be written as

$$S_{bis}(\alpha, \theta) = l_{PSM}(\alpha \cos\theta) S. \quad \text{(A11)}$$

Substituting (3) into (A11), the full polarimetric components can be expressed as

$$S_{hh,bis}(\alpha, \theta) = -l_{PSM}(\alpha \cos\theta) S_{dih} \cos 2\theta \quad \text{(A12)}$$

$$S_{hv,bis}(\alpha, \theta) = l_{PSM}(\alpha \cos\theta) S_{dih} \sin 2\theta \quad \text{(A13)}$$

$$S_{vh,bis}(\alpha, \theta) = l_{PSM}(\alpha \cos\theta) S_{dih} \sin 2\theta \quad \text{(A14)}$$

$$S_{vv,bis}(\alpha, \theta) = l_{PSM}(\alpha \cos\theta) S_{dih} \cos 2\theta \quad \text{(A15)}$$

where

$$l_{PSM}(\alpha \cos\theta) = \left|\cos(\alpha \cos\theta) \frac{\sin[k\sqrt{2}w \sin(\alpha \cos\theta)]}{k\sqrt{2}w \sin(\alpha \cos\theta)}\right|. \quad \text{(A16)}$$

As α is small in amount, we have $\cos(\alpha \cos\theta) \approx 1$, $\sin(\alpha \cos\theta) \approx \alpha \cos\theta$, and

$$l_{PSM}(\alpha \cos\theta) \approx \left|\frac{\sin(k\sqrt{2}w\alpha \cos\theta)}{k\sqrt{2}w\alpha \cos\theta}\right|. \quad \text{(A17)}$$

Suppose that $k\sqrt{2}\ w\alpha < \pi$, ignore the variance of θ, there are

$$l_{PSM}(\alpha \cos\theta) \approx \frac{\sin(k\sqrt{2}w\alpha \cos\theta)}{k\sqrt{2}w\alpha \cos\theta}. \quad \text{(A18)}$$

Considering the Taylor's expansion of $\sin x = x - (1/3!)x^3 + \cdots$, it can be approximated to

$$l_{PSM}(\alpha \cos\theta) \approx 1 - \frac{1}{3!}(k\sqrt{2}w\alpha \cos\theta)^2 \quad \text{(A19)}$$

or

$$l_{PSM}(\alpha \cos\theta) \approx 1 - 2A_1 \cos^2\theta \quad \text{(A20)}$$

where $A_1 = (1/3!)(kw\alpha)^2$.

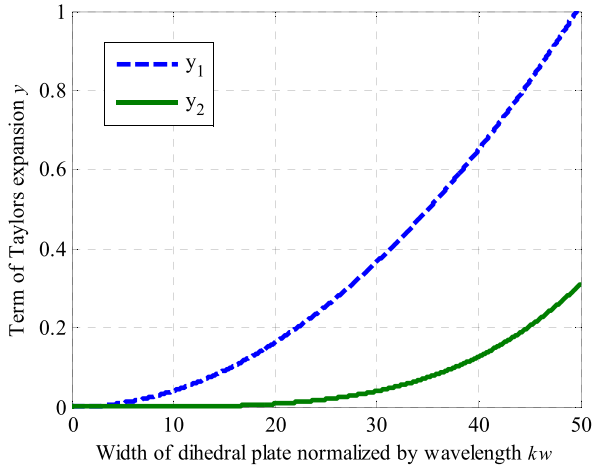

Fig. 16. Terms of Taylor's expansion varying with the width of dihedral plate.

The approximation we used depends on the factor $k\sqrt{2}\ w\alpha$. Fig. 16 demonstrates the terms $y_1 = (1/3!)(k\sqrt{2}\ w\alpha)^2$ and $y_2 = (1/5!)(k\sqrt{2}\ w\alpha)^4$ varying with the width of dihedral plate normalized by wavelength kw when the bistatic angle α is 2°. It can be seen that y_2 is small enough to be ignored.

Substituting (A20) into the full polarimetric components and taking vv component as an example of copolarization and hv component as an example of cross-polarization, the results are

$$S_{vv,bis}(\alpha, \theta) = S_{dih}\left[-\frac{A_1}{2} + (1 - A_1)\cos 2\theta - \frac{A_1}{2}\cos 4\theta\right] \quad \text{(A21)}$$

$$S_{hv,bis}(\alpha, \theta) = S_{dih}\left[(1 - A_1)\sin 2\theta - \frac{A_1}{2}\sin 4\theta\right]. \quad \text{(A22)}$$

The quasi-monostatic result of vv component is combined by $\cos 2\theta$, $\cos 4\theta$, and constant components and the hv component is combined by $\sin 2\theta$ and $\sin 4\theta$ components. The variants of c_2 and s_2 can be represented as

$$\frac{S_{vv,bis}(\alpha, 0) - S_{vv,bis}\left(\alpha, \frac{\pi}{2}\right)}{S_{dih}} = 2(1 - A_1) = l_{PSM}(\alpha) + 1 \quad \text{(A23)}$$

$$\frac{S_{hv,bis}\left(\alpha, \frac{\pi}{4}\right)}{S_{dih}} = 1 - A_1 = l_{PSM}\left(\alpha \cos\frac{\pi}{4}\right). \quad \text{(A24)}$$

The dihedral responses with quasi-monostatic geometry can be written as

$$S_{vv,bis} = \frac{l_{PSM}(\alpha) + 1}{2} S_{dih} \cos 2\theta \quad \text{(A25)}$$

$$S_{hv,bis} = l_{PSM}\left(\alpha \cos\frac{\pi}{4}\right) S_{dih} \sin 2\theta. \quad \text{(A26)}$$

What is more, if the term $y_2 = (1/5!)(k\sqrt{2}\ w\alpha)^4$ cannot be ignored and must be kept in the approximation of (A18), there will be $\cos 6\theta$ component in vv and $\sin 6\theta$ component in hv results. The simplified results of dihedral responses with quasi-monostatic geometry in this situation may be analyzed similarly.

REFERENCES

[1] W. Wiesbeck and S. Riegger, "A complete error model for free space polarimetric measurements," *IEEE Trans. Antennas Propag.*, vol. 39, no. 8, pp. 1105–1111, Aug. 1991.

[2] W. Wiesbeck and D. Kahny, "Single reference, three target calibration and error correction for monostatic, polarimetric free space measurements," *Proc. IEEE*, vol. 79, no. 10, pp. 1551–1558, Oct. 1991.

[3] K. Sarabandi and F. T. Ulaby, "A convenient technique for polarimetric calibration of single-antenna radar systems," *IEEE Trans. Geosci. Remote Sens.*, vol. 28, no. 6, pp. 1022–1033, Nov. 1990.

[4] A. Nashashibi, K. Sarabandi, and F. T. Ulaby, "A calibration technique for polarimetric coherent-on-receive radar systems," *IEEE Trans. Antennas Propag.*, vol. 43, no. 4, pp. 396–404, Apr. 1995.

[5] T.-J. Chen, T.-H. Chu, and F.-C. Chen, "A new calibration algorithm of wide-band polarimetric measurement system," *IEEE Trans. Antennas Propag.*, vol. 39, no. 8, pp. 1188–1192, Aug. 1991.

[6] C. M. H. Unal, R. J. Niemeijer, J. S. van Sinttruyen, and L. P. Ligthart, "Calibration of a polarimetric radar using a rotatable dihedral corner reflector," *IEEE Trans. Geosci. Remote Sens.*, vol. 32, no. 4, pp. 837–845, Jul. 1994.

[7] L. A. Muth, "Polarimetric calibration of indoor and outdoor polarimetric radar cross section systems," in *Proc. Antenna Meas. Techn. Assoc. (AMTA)*, Boston, MA, USA, Nov. 2008, pp. 37–42.

[8] L. A. Muth, "Nonlinear calibration of polarimetric radar cross section measurement systems," *IEEE Antennas Propag. Mag.*, vol. 52, no. 3, pp. 187–192, Jun. 2010.

[9] J.-R. J. Gau and W. D. Burnside, "New polarimetric calibration technique using a single calibration dihedral," *IEE Proc. Microw., Antennas Propag.*, vol. 142, no. 1, pp. 19–25, Feb. 1995.

[10] B. M. Welsh, B. M. Kent, and A. L. Buterbaugh, "Full polarimetric calibration for radar cross-section measurements: Performance analysis," *IEEE Trans. Antennas Propag.*, vol. 52, no. 9, pp. 2357–2365, Sep. 2004.

[11] R. E. Kell, "On the derivation of bistatic RCS from monostatic measurements," *Proc. IEEE*, vol. 53, no. 8, pp. 983–988, Aug. 1965.

[12] W. Anderson, "Consequences of nonorthogonality on the scattering properties of dihedral reflectors," *IEEE Trans. Antennas Propag.*, vol. AP-35, no. 10, pp. 1154–1159, Oct. 1987.

[13] K. J. Harker, "Backscattering by right-angle dihedrals for all possible angles of incidence," *IEEE Trans. Antennas Propag.*, vol. AP-61, no. 7, pp. 3739–3746, Jul. 2013.

[14] J. A. Jackson, "Closed-form, bistatic, 3D scattering solution for a dihedral corner reflector," in *Proc. Progr. Electromagn. Res. Symp. (PIERS)*, vol. 6, no. 5, pp. 495–499, Jan. 2010.

[15] A. Tempelis, M. Jussaume, and J. A. Jackson, "Comparison of measured and predicted bistatic scattering from a right-angle dihedral," in *Proc. IEEE Radar Conf.*, Kansas City, MO, USA, May 2011, pp. 135–140.

[16] C. Beaudoin, T. Horgan, G. Demartinis, M. J. Coulombe, A. J. Gatesman, and W. E. Nixon, "Fully polarimetric bistatic radar calibration with modified dihedral objects," *IEEE Trans. Antennas Propag.*, vol. 66, no. 2, pp. 937–950, Feb. 2018.

[17] R. J. Burkholder, "Analytic solutions for the bistatic radar signature of a dihedral target of arbitrary angle," *Int. Appl. Comput. Electromagn. Soc. Symp. (ACES)*, Denver, CO, USA, Mar. 2018, pp. 1–2.

[18] P. Wu and X. Xu, "A correction formulation for RCS measurement of dihedral reflector with quasi-monostatic geometry," in *Proc. Int. Conf. Electromagn. Adv. Appl. (ICEAA)*, Cairns, QLD, Australia, Sep. 2016, pp. 381–384.

[19] J. A. Jackson, "Analytic physical optics solution for bistatic, 3D scattering from a dihedral corner reflector," *IEEE Trans. Antennas Propag.*, vol. 60, no. 3, pp. 1486–1495, Mar. 2012.

[20] H. B. Song, K. Ji, K. Yang, H. Zou, and J. Mo, "Extension of analytic physical optics to calculate bistatic 3D scattering from obtuse dihedral," *J. Electromagn. Waves Appl.*, vol. 31, no. 13, pp. 1304–1324, Jul. 2017.

[21] E. F. Knott, "Calibration," in *Radar Cross Section Measurements*. New York, NY, USA: Van Nostrand Reinhold, 1993, pp. 183–187.

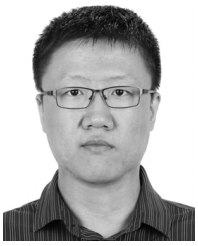

Pengfei Wu was born in Beijing, China, in 1988. He received the B.S. degree in electronic information and control engineering from the Beijing University of Technology, Beijing, in 2010. He is currently pursuing the Ph.D. degree in signal and information processing with the School of Electronics and Information Engineering, Beihang University, Beijing.

His current research interests include radar cross section (RCS) measurement and polarimetric calibration.

Xiaojian Xu was born in Wanan, Jiangxi, China, in 1963. He received the B.S. degree in electrical engineering from the Hefei University of Technology, Hefei, China, in 1983, the M.S. degree in electrical engineering from the Beijing Institute of Environmental Features (BIEF), Beijing, China, in 1986, and the Ph.D. degree in electrical engineering from the University of Nebraska–Lincoln, Lincoln, NE, USA, in 2002.

From 1986 to 1999, he was with BIEF, where he was involved in the research of electromagnetic scattering modeling and microwave imaging. From 1999 to 2002, he was with the Environmental Remote Sensing Laboratory, University of Nebraska–Lincoln, where he was involved in the research work on ultrawideband random noise radar, with emphasis on foliage and ground-penetration applications. Since 2003, he has been a Professor of signal and information processing with the School of Electronics and Information Engineering, Beihang University, Beijing. His current research interests include remote sensing signatures, radar imagery, target recognition, and system modeling.